Journal of Zhejiang University-SCIENCE C (Computers & Electronics)
ISSN 1869-1951 (Print); ISSN 1869-196X (Online)
www.zju.edu.cn/jzus; www.springerlink.com
E-mail: jzus@zju.edu.cn

# An extended processing scheme for coherent integration and parameter estimation based on matched filtering in passive radar

Xin GUAN[†1,2,3], Li-hua ZHONG[1,2], Dong-hui HU[1,2], Chi-biao DING[2]

([1]*Key Laboratory of Technology in Geo-spatial Information Processing and Application System, Beijing 100190, China*)

([2]*Institute of Electronics, Chinese Academy of Sciences, Beijing 100190, China*)

([3]*University of Chinese Academy of Sciences, Beijing 100190, China*)

[†]E-mail: xinguanxin@126.com

Received Mar. 6, 2014; Revision accepted June 23, 2014; Crosschecked Oct. 20, 2014

**Abstract:** In passive radars, coherent integration is an essential method to achieve processing gain for target detection. The cross ambiguity function (CAF) and the method based on matched filtering are the most common approaches. The method based on matched filtering is an approximation to CAF and the procedure is: (1) divide the signal into snapshots; (2) perform matched filtering on each snapshot; (3) perform fast Fourier transform (FFT) across the snapshots. The matched filtering method is computationally affordable and can offer savings of an order of 1000 times in execution speed over that of CAF. However, matched filtering suffers from severe energy loss for high speed targets. In this paper we concentrate mainly on the matched filtering method and we use keystone transform to rectify range migration. Several factors affecting the performance of coherent integration are discussed based on the matched filtering method and keystone transform. Modified methods are introduced to improve the performance by analyzing the impacts of mismatching, precision of the keystone transform, and discretization. The modified discrete chirp Fourier transform (MDCFT) is adopted to rectify the Doppler expansion in a multi-target scenario. A novel velocity estimation method is proposed, and an extended processing scheme presented. Simulations show that the proposed algorithms improve the performance of matched filtering for high speed targets.

**Key words:** Keystone transform, Matched filtering, MDCFT, Mismatching, Passive radar, Velocity estimation
**doi:**10.1631/jzus.C1400074 **Document code:** A **CLC number:** TN958.97

## 1 Introduction

Passive bistatic radar (PBR) is a kind of system using illuminators of opportunity to detect moving targets. In the past two decades, there has been a growing interest in this type of system (Howland, 2005; Griffiths, 2011). PBR has advantages including low-cost, no need for additional frequency allocation, and the merit of being undetectable, since the illuminator is not a part of the system. Many universities and institutes have conducted experiments and studies to investigate or improve the system performance (Howland *et al.*, 2005; Celik *et al.*, 2011; Palmer *et al.*, 2011), especially for the PBR based on digital signals (Yardley, 2007; Palmer *et al.*, 2013; Zhao *et al.*, 2013).

At least two antennas are required in PBR. The echo antenna collects the target signal as well as the direct signal and clutter. Meanwhile, the reference antenna collects only the direct signal. The direct signal and clutter in the echo channel can be removed by adaptive interference cancelation (Cherniakov, 2008). However, the target signal is usually weaker than noise. Therefore, coherent integration is necessary to improve the signal-to-noise ratio (SNR). Passive coherent location (PCL) is usually employed to perform coherent integration in PBR. The cross ambiguity function (CAF) and the method based on matched filtering (Cherniakov, 2008; Berger *et al.*, 2010) are two typical methods to implement PCL. In CAF, the echo signal is cross-correlated with the

Doppler-shifted copies of the reference signal. In matched filtering based coherent integration, a number of data snapshots are calculated by dividing the signal into segments, and matched filtering is performed for each snapshot. Then the Fourier transform is performed across snapshots to determine the Doppler shifts. Sampled points within each snapshot (resp. across snapshots) are called 'range cells' (resp. 'Doppler cells'). The output of CAF or the matched filtering of a target is a sinc-like peak. We use 'integration energy' to represent the power of the integration peak in our work, since the power of the peak represents the integration performance.

Unfortunately PCL suffers from energy loss when targets are moving at high speed, because high speed targets usually move from one range cell to another during the integration time, resulting in decreased integration energy. The phenomenon is the so-called 'range migration'. Moreover, the bistatic geometry changes when the target moves from one position to another. Hence, the bistatic Doppler frequency is varying with time, which is called 'Doppler expansion' (Malanowski *et al.*, 2011). Doppler expansion also results in energy loss. The loss is more serious for passive radar as the transmit signal is continuous and is different from chirp signal (discussed in Section 3). For CAF, range migration can be rectified by using keystone transform (Liu *et al.*, 2011) or modified ambiguity (Malanowski *et al.*, 2011), which changes the scale of the complex envelope. Then the fractional Fourier transform (FRFT) or the convolution with an impulse response is used to remove the Doppler expansion (Liu *et al.*, 2011; Malanowski, 2012). However, CAF is not suitable for real-time processing since the cross-correlation between the echo signal and the Doppler-shifted copies of the reference signal results in high complexity. If the data length is $N$ and the number of range cells to be calculated is $L$, then the number of complex multiplications is $L\times(N+N/2\times\log_2 N)$.

The procedure of matched filtering is (Cherniakov, 2008): (1) divide the signal into snapshots; (2) perform matched filtering on each snapshot; (3) perform fast Fourier transform (FFT) across the snapshots. The matched filtering can be implemented by FFT: (1) perform FFT over each snapshot of the echo and the reference signal; (2) perform conjugate multiplication between the processed echo and reference signal; (3) perform inverse FFT (IFFT) over each snapshot. If $M$ snapshots are formed, the number of complex multiplications is $M\times(L+3L/2\times\log_2 L)+L\times M\times\log_2 M$, where $M$ and $L$ are far less than $N$. Therefore, matched filtering takes less time than CAF. Normally matched filtering can offer savings of an order of 1000 times in execution time.

In our work, we focus on matched filtering to reduce the cost. In addition, keystone transform (Li *et al.*, 2006) is used to rectify range migration, which changes the scale of the complex envelope to remove the varying envelope caused by the motion of targets. The problems of energy loss and parameter estimation based on matched filtering and keystone transform are the main topics in our work.

By analyzing the signal model of the output of matched filtering and keystone transform in Section 2, we can summarize that there are four main factors affecting energy loss (we call the loss of the power of the target peak 'energy loss'). The four factors are mismatching, precision of the keystone implementation methods, discretization, and Doppler expansion. We make a theoretical study focusing on these four factors and present an integrated signal processing scheme to improve the performance of coherent integration in passive radars.

Mismatching is introduced by the approximation of no phase rotation within each snapshot (Petri *et al.*, 2012). The frequency spectrum of the echo snapshot is not the same as that of the reference snapshot because of the phase rotation introduced by the speed of targets. Hence, energy loss of matched filtering occurs, since the output of matched filtering achieves the highest power when the frequency spectrum is the same as that of the reference signal. In our work, we find that the Doppler filter banks can be a possible solution.

We take the impact of the precision of the keystone transform and the discretization into consideration, since they have not been analyzed before for PBR. The keystone transform is adopted here to rectify range migration and there are several implementation methods for the keystone transform with different processing errors. The higher the error is, the lower the performance of the keystone transform is. We call this impact the precision of the keystone transform. Further explanations are presented in Section 2. By comparing the principle of different

keystone methods, a better implementation method is selected. Moreover, the discretization affects the integration results and we will show that the interpolation can improve the performance.

As to the Doppler expansion, a compensation method based on the modified discrete chirp Fourier transform (MDCFT) is adopted. MDCFT removes the Doppler expansion by the estimate of the changing rate of the Doppler frequency. The distribution area of the sidelobes is analyzed for better detection in a multi-target scenario, which has not been discussed for PBR in the existing methods. At last, a velocity estimation method using one receiver is proposed based on the estimated changing rate of Doppler to improve the parameter estimation performance.

Various methods have been proposed to improve the performance considering the four factors, forming an extended processing scheme, and this is the main contribution of our work.

## 2 Analyses of energy loss based on matched filtering and keystone transform

In PBR systems, the transmitter and the receiver are located separately (Fig. 1).

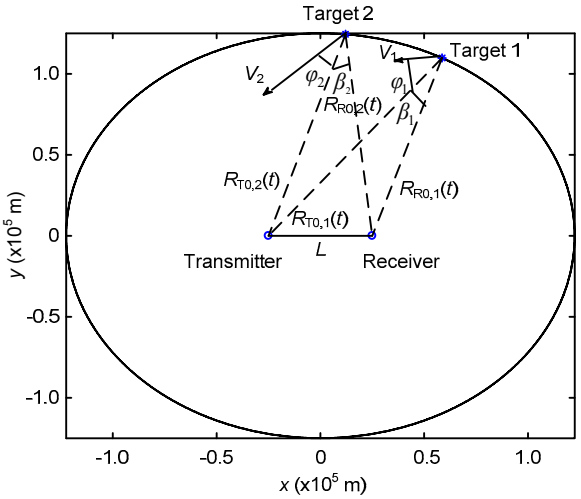


**Fig. 1 The bistatic setup of passive bistatic radar (PBR)**

The illuminator transmits continuous waveform. The baseband signal is represented as $s(t)$. For the PBR based on the digital television signal, frequency modulated (FM) signal, or other communication signals, the signal on the radio frequency (RF) is

$$x(t)=\mathrm{Re}\{s(t)\exp(\mathrm{j}2\pi f_c t)\}, \tag{1}$$

where $f_c$ is the carrier frequency, and $t$ is the continuous time. After down-conversion of the RF signal, the echo signal $S_{\mathrm{echo}}(t)$ and reference signal $S_{\mathrm{ref}}(t)$ are

$$\begin{aligned}S_{\mathrm{echo}}(t)=&\sum_i\left[A_i(t)\exp(\mathrm{j}\theta_i(t))s(t-R_i(t)/c)\right.\\&\left.\cdot\exp(-\mathrm{j}2\pi f_c R_i(t)/c)\right]+w_1(t),\end{aligned} \tag{2}$$

$$S_{\mathrm{ref}}(t)=A_r s(t)+w_2(t), \tag{3}$$

where $R_i(t)$, $A_i(t)$, and $\theta_i(t)$ denote the bistatic range, amplitude, and phase of the $i$th target, respectively. The constant $c$ represents the speed of light and $A_r$ is the amplitude of the reference signal. The notations $w_1(t)$ and $w_2(t)$ denote the noises. The variable $\theta_i(t)$ is affected by many factors, such as the material of the targets, the flight attitude of aircrafts, and even the environment. For simplicity, we assume that there is no amplitude or phase fluctuation during the integration time. Then $A_i(t)\exp(\mathrm{j}\theta_i(t))$ can be simplified to an unknown constant $A_i$. Note that $s(t)$, $w_1(t)$, and $w_2(t)$ are independent; therefore, we ignore $w_1(t)$ and $w_2(t)$ in the following equations for simplicity. According to Fig. 1, the bistatic range is described as

$$\begin{aligned}R_i(t)=&\sqrt{R_{\mathrm{T0},i}^2+v_i^2t^2-2R_{\mathrm{T0},i}v_it\cos\varphi_i}\\&+\sqrt{R_{\mathrm{R0},i}^2+v_i^2t^2-2R_{\mathrm{R0},i}v_it\cos(\varphi_i+\beta_i)}-L,\end{aligned} \tag{4}$$

where $L$, $R_{\mathrm{T0},i}$, $R_{\mathrm{R0},i}$, $v_i$, $\beta_i$, and $\varphi_i$ denote the length of the baseline, the distance between the target and illuminator, the distance between the target and receiver, the speed of the target, the bistatic angle, and the angle of the moving direction and the connection of the target and illuminator, respectively. Subscript $i$ denotes the $i$th target. The normal processing scheme of the matched filtering method and keystone transform is shown in Fig. 2.

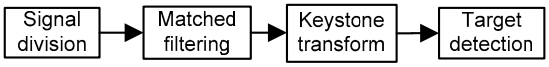


**Fig. 2 The normal processing scheme of the matched filtering method and keystone transform**

Analyses about the signal model under matched filtering and the keystone transform are as follows:

First, the signal is divided into snapshots. Then the discrete form is written as

$$S_{\text{echo}}(n,m)=\sum_i\big[A_i s(n\Delta t-R_i(n,m)/c,m)\cdot\exp(-\text{j}2\pi f_c R_i(n,m)/c)\big]+w_1(n,m), \tag{5}$$

$$S_{\text{ref}}(n,m)=A_r s(n,m)+w_2(n,m), \tag{6}$$

where $\Delta t$ is the sampling interval, and $n$ and $m$ represent 'fast-time' and 'slow-time' in discretized data space, respectively. Then

$$R_i(n,m)=\sqrt{R_{\text{R0},i}^2+v_i^2t^2(n,m)-2R_{\text{R0},i}v_it(n,m)\cos(\varphi_i+\beta_i)}+\sqrt{R_{\text{T0},i}^2+v_i^2t^2(n,m)-2R_{\text{T0},i}v_it(n,m)\cos\varphi_i}-L, \tag{7}$$

where $t(n, m)=mT+n\Delta t$. The duration of one snapshot of the reference signal is denoted by $T$. Apply the Taylor expansion to $R_i(n, m)$, and take the first- and second-order terms into consideration. Then the bistatic range is

$$R_i(n,m)=R_{\text{T0},i}+R_{\text{R0},i}-L-2v_{\text{r},i}\cos(\beta_i/2)(mT+n\Delta t)+\frac{1}{2}\left(\frac{\sin^2\varphi_i}{R_{\text{T0},i}}+\frac{\sin^2(\varphi_i+\beta_i)}{R_{\text{R0},i}}\right)v_i^2(mT+n\Delta t)^2, \tag{8}$$

where $v_{\text{r},i}=v_i\cos(\varphi_i+\beta_i/2)$. In addition, the impact of $n\Delta t$ on the second-order term can be ignored since it has less impact compared with $mT$.

If matched filtering is performed, according to Eqs. (5) and (8), the output of the filter in the frequency domain can be derived as

$$r(f,m)=\sum_i A_i'\,s\big(f-4\pi f_c v_{\text{r},i}\cos(\beta_i/2)/c,m\big)\cdot\text{conj}(s(f,m))\cdot\exp\big(-\text{j}2\pi f(R_{\text{T0},i}+R_{\text{R0},i}-L)/c\big)\cdot\exp\big(\text{j}4\pi(f+f_c)v_{\text{r},i}\cos(\beta_i/2)mT/c\big)\cdot\exp\left(-\text{j}\frac{2\pi f_c}{c}\left(\frac{v_i^2\sin^2\varphi_i}{2R_{\text{T0},i}}+\frac{v_i^2\sin^2(\varphi_i+\beta_i)}{2R_{\text{R0},i}}\right)(mT)^2\right), \tag{9}$$

where $A_i'=A_i\exp(-\text{j}2\pi f(R_{\text{T0},i}+R_{\text{R0},i}-L)/c)$, $f$ is the frequency, and 'conj' means 'conjugate'.

It can be seen from Eq. (9) that there are four factors leading to energy loss in the matched filtering method:

1. The range variation within each snapshot results in mismatching as presented in the expression $s(f-4\pi f_c v_{\text{r},i}\cos(\beta_i/2)/c,\ m)\cdot\text{conj}(s(f,\ m))$. This is introduced by the assumption of a constant Doppler (Petri *et al.*, 2012). In our analyses, we use the word 'mismatching' to describe this problem.

2. The expression $\exp(\text{j}4\pi(f+f_c)v_{\text{r},i}\cos(\beta_i/2)mT/c)$ changes with $m$ introducing range migration, and can be rectified by the keystone transform (Zhu *et al.*, 2007). The keystone transform is a scale changing operation on slow-time. The expression of the keystone transform for the continuous signals is $t_k=f_c t_m/(f_c+f)$, where $t_m$ is the slow time and $t_k$ is the time after the transform. For discrete signals, some implementation methods should be used to solve the problem (described later). However, the precision of the keystone implementation method has an influence on the performance, which should be taken into consideration as presented in the following analyses.

3. Discretization has an impact on the amplitude of the integration peak, since the value of the target peak may not be sampled from the highest point of the main peak because of discretization. Thereby, the influence of the discretization should also be taken into account.

4. Doppler expansion is introduced by $\exp\left(-\text{j}\frac{2\pi f_c v_i^2}{c}\left(\frac{\sin^2\varphi_i}{2R_{\text{T0},i}}+\frac{\sin^2(\varphi_i+\beta_i)}{2R_{\text{R0},i}}\right)(mT)^2\right)$. The phenomenon of Doppler expansion affects not only integration energy but also parameter estimation, such as the bistatic Doppler. One can obtain the bistatic speed $v_{\text{r},i}$ from the Doppler measurement in PBR. However, $v_i$ cannot be achieved by a single integration result in the literature. In the following, a method for estimating $v_i$ is proposed based on Doppler expansion.

In our work, the methods to improve the performance are proposed considering the four factors and this is the main contribution of this study. In Petri *et al*. (2012), mismatching has been analyzed, but we have shown here that the Doppler filter banks can be a solution to reduce the amount of energy loss. Among the four factors, the impacts of the precision of the keystone transform and the discretization have not

been analyzed in the literature. A more suitable keystone method has been selected to reduce the impact by analyses of the principles of different keystone transform implementation methods. The interpolation can also be used to reduce the loss introduced by discretization. Besides, MDCFT is used to compensate for the Doppler expansion. The resolution and parameter estimation performance, however, need further analyses in the multi-target scenario. Therefore, expressions about resolution are derived and analyses about estimation performance provided. An estimation method is then proposed to estimate the moving speed of the targets, differing from the bistatic speed in the literature about PBR. Finally, an extended processing scheme is formed considering all the improvements. The four factors and the corresponding solutions are discussed in detail in the following sections.

## 3 Analyses and improvement of mismatching, precision of the keystone transform and discretization

### 3.1 Mismatching

In Section 2, we have presented that mismatching occurs within each snapshot based on the signal model. The main reason is that a phase bias $4\pi f_c v_{r,i}\cos(\beta_i/2)/c$ is introduced by $4\pi f_c v_{r,i}\cos(\beta_i/2)\cdot n\Delta t/c$ in Eq. (8). The integration energy decreases because of the phase bias, since matched filtering achieves the highest output power only when $s(f-4\pi f_c v_{r,i}\cos(\beta_i/2)/c,\ m)\cdot\mathrm{conj}(s(f,\ m))$ simplifies to $s(f,\ m)\cdot\mathrm{conj}(s(f,\ m))$. In addition, the mismatching becomes more serious and the output of matched filtering reduces with the increase of $v_{r,i}$. Hence, the phase which is exactly equal to $4\pi f_c v_{r,i}\cos(\beta_i/2)n\Delta t/c$ is required to be multiplied with the echo snapshots, to eliminate the phase bias before matched filtering.

However, the target speed is always unknown in practice. Thereby, the phase bias cannot be totally removed. In this section, we propose a compensation method based on Doppler filter banks in which the signal presented in Eq. (5) is multiplied by phase $\varphi$ for each snapshot:

$$\varphi=\exp(-\mathrm{j}4\pi f_c v_c n\Delta t/c), \tag{10}$$

where $v_c\in[v_{\min}, v_{\max}]$, $v_{\min}$ and $v_{\max}$ are chosen based on the minimum and maximum speeds of the targets, respectively. If $v_c=v_{r,i}\cos(\beta_i/2)$, the mismatching can be totally compensated. Nevertheless, it is difficult to obtain the prior information of targets. Hence, the range of speed $[v_{\min}, v_{\max}]$ is discretized uniformly and each $v_k=v_{\min}+k\Delta v$ is adopted to perform the compensation, which can be called Doppler filter banks. The notation $\Delta v$ denotes the interval of the discretized speed.

This method is not an exact compensation. The remnant energy loss is determined by the difference between $v_{r,i}$ and $v_k$. The remnant expression of the mismatching is $s(f-4\pi f_c v_{r,i}\cos(\beta_i/2)/c,\ m)\times\mathrm{conj}(s(f,\ m))$. The energy loss is reduced, since $(v_{r,i}-v_k)$ is much smaller than $v_{r,i}$. The compensation result changes for different $k$ and $\Delta v$. In Section 5 the performance of Doppler filter banks is presented for the digital television signal based PBR.

Sometimes the Doppler ambiguity occurs in the matched filtering method. The following function is used before the keystone transform (Li *et al*., 2006) to solve the ambiguity:

$$\begin{aligned} r_k(f,m)&=\exp(-\mathrm{j}2\pi k f_r f_c mT/(f_c+f))r(f,m)\\ &=\exp(-\mathrm{j}2\pi k f_c m/(f_c+f))r(f,m), \end{aligned} \tag{11}$$

where $r_k(f, m)$ denotes the output of the matched filtering method in the *f*-*m* domain for the *k*th ambiguity number, and $f_r=1/T$. If $T$ increases, the energy loss also increases. Hence, it is better to compensate for the loss and remove the ambiguity in this situation. The flow chart is shown in Fig. 3 for $k=3$. Data association is required at the end of the procedure.

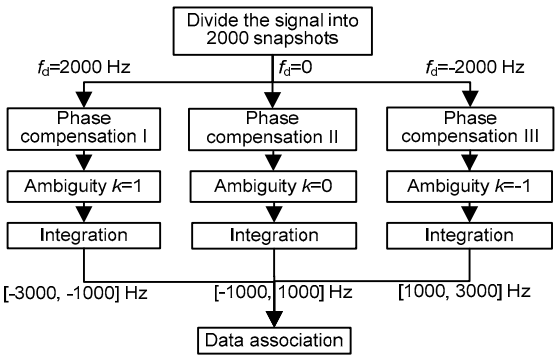


**Fig. 3 Phase compensation and ambiguity removal ($k$=3)**

### 3.2 Precision of the keystone transform

There are three types of methods to implement the keystone transform (Zhu *et al.*, 2007; Deng and Jiang, 2011): (1) Interpolation, e.g., sinc interpolation and linear interpolation. The precision of the interpolation affects the result of the keystone transform (Deng and Jiang, 2011). It is shown that using sinc is superior to using linear interpolation. (2) DFT+IFFT method. The computation burden of this method is huge for real-time processing systems. (3) Chirp-*z* method. FFT can be used for fast computation (Zhu *et al.*, 2007). However, the improvement of integration energy using this method has not been discussed. Work has been done to show the complexity of these methods in traditional radars. However, their impact on energy loss has not been carefully discussed.

In the expression of the keystone transform $t_k=f_c t_m/(f_c+f)$, time is presented in the continuous form. For the discrete form, the required values after scaling are calculated by interpolation. However, the processing precision is different for each method. For interpolation methods, the values after the keystone transform are estimated using different interpolation methods. However, there is difference between the ideal values and the calculated ones. Hence, there is energy loss if this kind of error occurs.

The realization procedure of chirp-*z* (Zhu *et al.*, 2007) is shown in Fig. 4. Suppose that $x_f(m)=r(f, m)$ for each $f$, $W=\exp(-j2\pi(f_c+f)/(Mf_c))$, and $A=1$. If the keystone transform is performed based on the chirp-*z* method, circular convolution is adopted to replace linear convolution according to Fig. 4. It can be seen that scaling is carried out along the unit circle in the *Z*-plane using all samples of the data. The required values after the scaling are directly calculated. Moreover, the chirp-*z* method avoids interpolation, which is an approximation to the real value, and thus more exact results can be achieved. Thereby, the chirp-*z* method not only is suitable for real-time processing, but also improves the precision of the keystone transform.

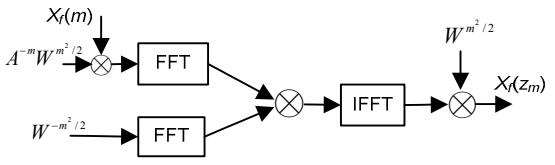


**Fig. 4 Keystone transform implemented based on chirp-*z***

For traditional radar systems, the transmitter launches chirp pulses. Each pulse has the same waveform. However, the continuous waveform is divided into snapshots on purpose in PBR. For instance, the digital television signal is a random-like sequence and has a noise-like spectrum. Therefore, the integration gain is more sensitive to the precision of the keystone transform compared with the traditional radars, and decreases rapidly with the decrease of $T$. The precision of the chirp-*z* method is better than those of the interpolation methods, such as sinc interpolation and linear interpolation. Thereby, the chirp-*z* method achieves better performance than the interpolation ones.

### 3.3 Discretization

Discretization is also an important factor resulting in decreased performance. If the real target occurs between two Doppler bins (resp. range bins), the highest point of the sinc-like peak may not just be sampled. In some traditional radar systems, this impact is not serious. However, the difference between the real value of the peak and the sampled point can be large and cannot be neglected in passive radar, because the main lobe of the target peak after integration is usually the thumbtack-like shape and the sampling rate is usually smaller than that in the radars using chirp pulses as the transmit signal.

We should mention that the sampling rate is higher than the Nyquist sampling rate in our cases. The problem of discretization is that the highest point of the main peak has not been sampled. Therefore, the maximum loss of SNR is related to the resolution and the sampling rate. For the digital television signal, the bandwidth is around 8 MHz. The resolution is 1/(8 MHz), which means a range resolution of $1.25\times10^{-7}$ m. When the sampling rate is also 8 MHz, the difference between the nearest range cells is also $1.25\times10^{-7}$ m. This means that the maximum loss is 3 dB, if the sampled point of the target peak is equal to the 3 dB width of the sinc-like peak. The loss decreases with the increase of the sampling rate.

Interpolation can be adopted to improve the chance of increased performance since the sampling rate is higher than the Nyquist sampling rate. If the sampled point is nearer to the real position than the previous one, the SNR is higher. However, the interpolation increases the amount of data and leads to

higher complexity. Therefore, the interpolation should be considered according to the real-time processing requirement. This is effective even in a noisy environment, which will be presented in Section 5.

## 4 Compensation for Doppler expansion and velocity estimation

### 4.1 Compensation by MDCFT

In this section we define

$$\begin{aligned} f_{\mathrm{d},i} &= 2v_{\mathrm{r},i}\cos(\beta_i/2)/\lambda \\ &= 2v_i\cos(\varphi_i+\beta_i/2)\cos(\beta_i/2)/\lambda, \end{aligned} \tag{12}$$

$$K_i = \frac{1}{\lambda}\left(\frac{v_i^2\sin^2\varphi_i}{R_{\mathrm{T0},i}}+\frac{v_i^2\sin^2(\varphi_i+\beta_i)}{R_{\mathrm{R0},i}}\right), \tag{13}$$

where $\lambda$ denotes the wavelength. According to Eq. (9), the signal after the compensation of mismatching and keystone transform is

$$\begin{aligned} r(n,m) = \sum_i \Big[ & A_i' s'(n-n_{0,i})\exp(-\mathrm{j}2\pi f_{\mathrm{d},i} mT) \\ & \cdot\exp(\mathrm{j}\pi K_i (mT)^2)\Big], \end{aligned} \tag{14}$$

where $n_{0,i}$ is the initial position of the $i$th target. It is proved in Eq. (14) that the signal is equivalent to a chirp signal centered at $f_{\mathrm{d},i}$, with the FM rate $K_i$.

If FFT is performed across the snapshots, the energy disperses along the Doppler cells. The methods for chirp signal detection can solve this problem. Several methods have been developed to detect chirp signals, including the Wigner-Ville distribution (WVD)-Hough transform (Barbarossa, 1995), FRFT (Dong *et al.*, 1999), and discrete chirp-Fourier transform (Xia, 2000). The WVD-Hough transform provides a good time and frequency resolution, but cross-terms may occur in a multi-target scenario. The reassigned smoothed pseudo WVD (RSPWVD) (Auger and Flandrin, 1995) can solve this problem; however, the computation complexity increases greatly. Therefore, the chirp-Fourier transform is designed particularly for chirp signal detection. The signal is multiplied by the chirp signals with a different FM rate and central frequency, and the results of the chirp-Fourier transform have no across terms. The discrete chirp-Fourier transform (DCFT) is the method for the discrete signal. However, DCFT achieves a good resolution only when the length of the signal is a prime number and both the central frequency and modulation frequency are integers (Xia, 2000). MDCFT (Guo *et al.*, 2002) has been developed to overcome the drawback of DCFT. The expression of MDCFT is

$$X_i(k,l)=\frac{1}{\sqrt{M}}\sum_{m=0}^{N-1}x_i(m)\exp\left(-\mathrm{j}\frac{2\pi km^2}{M^2}\right)\exp\left(-\mathrm{j}\frac{2\pi lm}{M}\right). \tag{15}$$

In our cases, $x_i(m)$ represents the signal extracted along each range cell, which is varying with the slow-time. The notations $k$ and $l$ are the discrete values based on all possible $K_i$ and $f_{\mathrm{d},i}$, which can be obtained by performing MDCFT. The scale of $K_i$ can be calculated according to Eq. (13) based on the maximum velocity to reduce the complexity.

In addition, the multi-target scenario should be considered especially for low resolution radars like PBR. For targets flying in a group, several targets may appear in the same range cell. The difference between the Doppler frequencies may not be large enough to separate them. MDCFT produces no cross-terms and is suitable for multi-target detection. The interval of the FM rate is usually small to improve the estimation precision. However, this results in high sidelobes (Fig. 5). Therefore, we have studied the distribution area of the sidelobes for better detection. The expressions about resolution are derived and the analyses about the performance of the estimation are provided. Moreover, an estimation method is proposed to estimate the speed of the targets (not the bistatic radial speed in the literature about PBR).

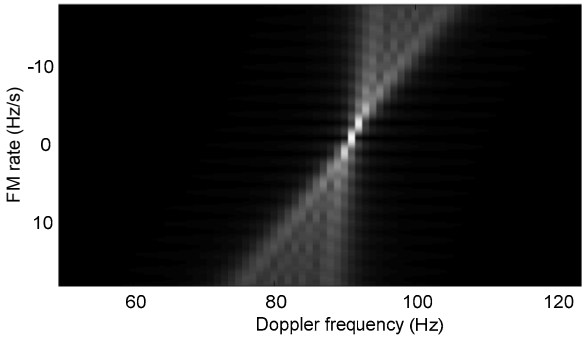


**Fig. 5 The distribution area of the sidelobes using MDCFT**

Define the signal to be detected as

$$x_i(m)=\exp(\mathrm{j}2\pi f_{\mathrm{d},i}m/M)\exp(-\mathrm{j}\pi K_i m^2/M^2). \tag{16}$$

Substituting Eq. (16) into Eq. (15) leads to

$$X_i(k,l)=\frac{1}{\sqrt{M}}\sum_{m=0}^{N-1}x_i(m)\exp\left(-\mathrm{j}\frac{2\pi lm}{M}\right)\exp\left(-\mathrm{j}\frac{2\pi km^2}{M^2}\right)$$
$$=\frac{1}{\sqrt{M}}\sum_{n=0}^{N-1}\exp\left(\mathrm{j}\frac{2\pi(f_{\mathrm{d},i}-(K_i-k)m/M)m}{M}\right)\exp\left(-\mathrm{j}\frac{2\pi lm}{M}\right). \tag{17}$$

Then the area of the sidelobes can be described as

$$\begin{aligned}&\text{Area}=f_{\mathrm{d},i}-(K_i-k)m/N,\\ &k\in[K_{\min},K_{\max}],\ m\in[0,M-1].\end{aligned} \tag{18}$$

MDCFT compensates for the term $\exp(\mathrm{j}\pi K_i t_{\mathrm{m}}^2)$ in Eq. (14); therefore, the Doppler shifts reduce to a single value determined by $f_{\mathrm{d},i}$ (the initial Doppler at the beginning of the integration time).

Note that MDCFT provides more information of velocity, which is an important parameter for target classification, and helps distinguish targets from interferences. However, the directly obtained speed is usually not the actual moving speed, but is related to bistatic speed $v_{\mathrm{r},i}$ and bistatic angle $\beta_i$. Multistatic setup or more data processing is required to estimate the $v_i$. In this section, the formulas of velocity estimation are derived based on the compensation method proposed above.

Define the angle of the baseline and the connection line of the $i$th target and the receiver as $\theta_{\mathrm{r},i}$. Then

$$R_{\mathrm{R}0,i}+R_{\mathrm{T}0,i}-L=n_{0,i}c/f_{\mathrm{s}}, \tag{19}$$
$$R_{\mathrm{T}0,i}^2=R_{\mathrm{R}0,i}^2+L^2-2R_{\mathrm{R}0,i}L\cos(\pi-\theta_{\mathrm{r},i}), \tag{20}$$

where $f_{\mathrm{s}}$ is the sampling rate. Hence,

$$R_{\mathrm{T}0,i}=\frac{2(n_{0,i}c/f_{\mathrm{s}}+L)L\cos(\pi-\theta_{\mathrm{r},i})-(n_{0,i}c/f_{\mathrm{s}}+L)^2-L^2}{2L\cos(\pi-\theta_{\mathrm{r},i})-2(n_{0,i}c/f_{\mathrm{s}}+L)}, \tag{21}$$
$$R_{\mathrm{R}0,i}=n_{0,i}c/f_{\mathrm{s}}+L-R_{\mathrm{T}0,i}, \tag{22}$$
$$\beta_i=\arcsin[L\sin(\pi-\theta_{\mathrm{r},i})/R_{\mathrm{T}0,i}]. \tag{23}$$

The notations $v_i$, $\beta_i$, and $\varphi_i$ can be worked out using the measurements of the azimuth. Let $v_{\mathrm{q},i}=v_i\sin(\varphi_i+\beta_i/2)$. Then

$$v_i=\sqrt{v_{\mathrm{q},i}^2+v_{\mathrm{r},i}^2}, \tag{24}$$
$$v_{\mathrm{q},i}=\frac{-a_{1,i}\pm\sqrt{a_{1,i}^2-4a_{2,i}a_{3,i}}}{2a_{2,i}}, \tag{25}$$

where

$$a_{2,i}=(R_{\mathrm{R}0,i}+R_{\mathrm{T}0,i})\cos^2(\beta_i/2), \tag{26}$$
$$a_{1,i}=v_{\mathrm{r},i}(R_{\mathrm{T}0,i}-R_{\mathrm{R}0,i})\sin\beta_i, \tag{27}$$
$$a_{3,i}=v_{\mathrm{r},i}^2\sin^2(\beta_i/2)(R_{\mathrm{R}0,i}+R_{\mathrm{T}0,i})-K_i\lambda R_{\mathrm{T}0,i}R_{\mathrm{R}0,i}. \tag{28}$$

Thereby, we can obtain a rough estimate of the moving speed of targets using a single receiver within the integration time using the proposed estimation method.

### 4.2 Extended processing scheme

The complete extended processing scheme discussed in Sections 3 and 4 is summarized in Fig. 6.

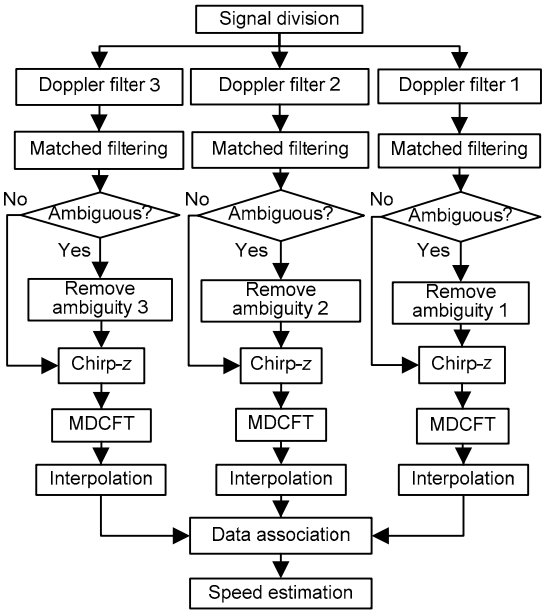


**Fig. 6 The extended processing scheme**

The duration of one snapshot of the reference signal should be chosen properly to determine whether the ambiguity removal is necessary. The results are associated after parallel processing and the maximum value should be selected as the final result for each target. Moreover, the number of filter banks should be selected based on the real-time processing requirements of the system.

## 5 Simulations

Simulations have been carried out to verify the effectiveness of the extended processing scheme. The

carrier frequency is 674 MHz. The transmit signal is the digital television terrestrial broadcasting (DTTB) signal (National Standardization Committee of China, 2006). The integration time is 1 s. The noise factor is 2 dB. The bistatic setup is selected according to the parameters commonly used in the literature. Two radar geometries are simulated. In case 1, the distance between the transmitter and the receiver is 50 km and the targets are about 100 km away from the receiver with an azimuth of 20°. In case 2, the distance between the transmitter and the receiver is 40 km and the targets are about 75 km away from the receiver with an azimuth of 30°.

It was proved in Section 2 that the mismatching and the precision of the keystone transform are affected mainly by the bistatic speed $v_{r,i}\cos(\beta_i/2)$. Meanwhile, the Doppler expansion is determined by $K_i=(v_i^2\sin^2\varphi_i/R_{T0,i}+v_i^2\sin^2(\varphi_i+\beta_i)/R_{R0,i})/\lambda$. Therefore, the proposed methods are designed based on $v_{r,i}\cos(\beta_i/2)$ and $K_i$. Hence, the simulations are carried out for different $v_{r,i}\cos(\beta_i/2)$ ($K_i$ is around zero) to analyze mismatching, precision of the keystone transform, and discretization. The Doppler expansion is analyzed for a fixed $v_{r,i}\cos(\beta_i/2)$ and different $K_i$ in these two cases.

### 5.1 Mismatching

In Section 3.1, the Doppler filter banks are designed to reduce the energy loss introduced by mismatching. Simulations are performed in this subsection to show the performance of Doppler filter banks.

First, simulations are carried out in case 1. The reference signal is divided into 6000 snapshots, and the length of the echo snapshot is set to 13 500 (cells) to provide unambiguous detection of targets with a maximum speed of 680 m/s. The simulated targets are with $v_{r,i}\cos(\beta_i/2)=(299.50, 399.33, 598.99)$ m/s and $K_i$ is around zero. Different values of the speed are selected to calculate $\varphi_i$, and the results of Doppler filter banks in case 1 are depicted in Fig. 7a. The maximum SNR of each curve is not the same, because of the unavoidable factors, such as discretization and noise. However, it can be concluded that the highest SNR is achieved around $v_c=v_{r,i}\cos(\beta_i/2)$ for each curve and the SNR decreases with the growth of the difference between $v_c$ and $v_{r,i}\cos(\beta_i/2)$. Therefore, if $v_c$ is chosen properly, the energy loss introduced by mismatching can be reduced.

Second, we select the number of snapshots as 2000 and the length of each echo snapshot as 16 500 (cells). The results for case 1 are shown in Fig. 7b. The number of snapshots is smaller compared with that in Fig. 7a. Thereby, the loss of mismatching is more severe and Doppler ambiguity may occur. The ambiguity number is $k=(-1, 0, 1)$. We use $v_c\in[220, 600]$ m/s to implement Doppler filter banks this time. The $v_c$ is chosen corresponding to the right ambiguity number. If ambiguity is not removed, then the target is buried in noise (Fig. 7c). If ambiguity is removed, the target can be detected (Fig. 7d). Hence, Doppler filter banks also work well as long as ambiguity has been removed.

Third, similar results are obtained for case 2 (Figs. 7e and 7f). Fig. 7e shows the performance with $v_{r,i}\cos(\beta_i/2)=(248.98, 448.17, 647.36)$ m/s and $K_i=0$, when the number of the snapshots is 6000. Results in Fig. 7f are obtained using $v_c\in[220, 650]$ m/s with ambiguity removal when the number of snapshots is 2000.

Finally, it can be concluded from both cases that the integration loss of the targets moving slower than 600 m/s can be controlled within 1 dB with the Doppler difference smaller than 1000 Hz (Figs. 7a, 7b, 7e, and 7f). This can be used for common cases. In our cases, $v_c=(2000, 0, 2000)$ Hz can be chosen to implement the Doppler filter banks.

In the above simulations, the energy loss increases with the decrease of the number of snapshots, but the computation complexity reduces. The execution time (C program, Intel Xeon CPU X5670, 20-core, parallel) for different numbers of snapshots is depicted in Table 1.

**Table 1 Execution time for different numbers of snapshots**

| Number of snapshots | 1000 | 2000 | 3000 | 6000 |
|---|---|---|---|---|
| Execution time (s) | 0.5609 | 0.9459 | 1.3922 | 2.7789 |

### 5.2 Precision of the keystone transform

Simulations have been carried out to show the impact of different implementation methods of the keystone transform on energy loss. $K$ is fixed to zero for the simulated targets. The SNR reduces with the increase of $v_{r,i}\cos(\beta_i/2)$ (Fig. 8), because of the mismatching discussed above. The results of cases 1 and 2 are presented in Figs. 8a and 8b, respectively.

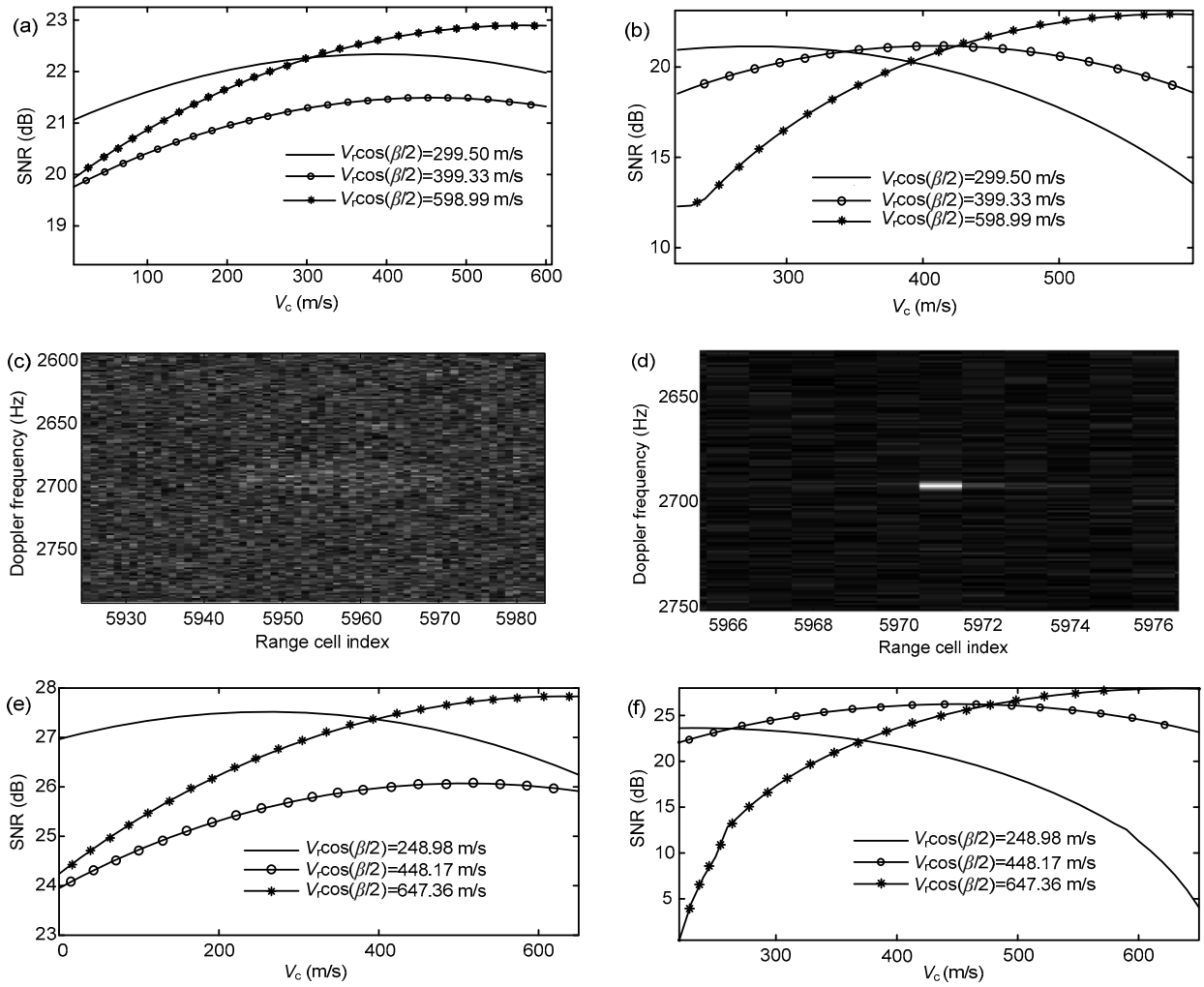


**Fig. 7 Results of the Doppler filter banks**

(a) Case 1: $v_c$ is varying from 0 to 600 m/s; (b) Case 1 with ambiguity removal when the snapshot number is 2000; (c) Result without ambiguity removal in case 1 for $v_{r,i}\cos(\beta_i/2)$=597.76 m/s; (d) Result with ambiguity removal in case 1 for $v_{r,i}\cos(\beta_i/2)$= 597.76 m/s; (e) Case 2: $v_c$ is varying from 0 to 650 m/s; (f) Case 2 with ambiguity removal when the snapshot number is 2000

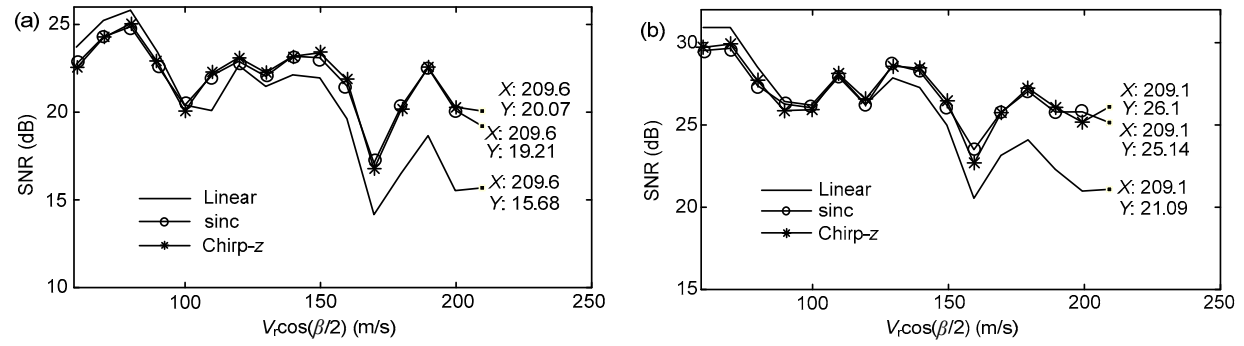


**Fig. 8 The SNR after the keystone transform for different implementation methods: (a) case 1; (b) case 2**

The SNR fluctuates along the curve because of the impact of noise. Fig. 8 shows that the amount of the energy loss increases with the increase of $v_{r,i}\cos(\beta_i/2)$ for these two cases, which means the impact of keystone precision is more obvious. The chirp-$z$ method and sinc interpolation show stable performance compared with linear interpolation.

Furthermore, the execution time of different approaches differs from each other. In Table 2 the processing time (MATLAB R2010a, no parallelism) is presented. The length of each echo snapshot is 18000 (cells). The results show that the sinc interpolation method is the slowest.

It can be concluded from the simulations that linear interpolation is the fastest with the worst precision, and that chirp-$z$ achieves higher precision with acceptable execution time. As the timing is also influenced by factors such as the resource schedule of the system and memory, the timing may be slightly non-linear with the number of snapshots. Hence, chirp-$z$ is more suitable for implementation of the keystone transform in passive radars.

**Table 2 Execution time for different keystone methods**

| Number of snapshots | Execution time (s) | | |
|---|---|---|---|
| | Linear | sinc | Chirp-$z$ |
| 1000 | 5.7721 | 213.0998 | 29.4695 |
| 2000 | 8.3823 | 428.1781 | 61.6649 |

### 5.3 Discretization

In Section 3.3, we have discussed the impact of discretization. The interpolation can improve the chance of increased performance, since the impact is introduced by discretization. If the sampled point is nearer to the real position than the previous one, the SNR is higher. As shown in Fig. 9, the SNR of the target after interpolation is sometimes higher than that before interpolation. Figs. 9a and 9b present the results in case 1, and Figs. 9c and 9d the results in case 2. The improvements for different targets are not the same since the energy loss introduced by discretization varies from 0 to over 3 dB along the range or Doppler cells. However, it can be seen from the figures that the interpolation can reduce the loss. Note that the losses of different target positions between the nearest two bins vary from each other from 0 to 3 dB; therefore, the improvement after interpolation also varies. Figs. 9e and 9f show the cross-section of the target with $v_{r,i}\cos(\beta_i/2)$=99.83 m/s in case 1.

### 5.4 Doppler expansion and velocity estimation

First, simulations are performed to analyze the algorithm proposed in Section 4. The target speed is set to 680 m/s with $v_{r,i}\cos(\beta_i/2)$=59.7764 m/s in case 1. The azimuth angle is 20°. Fig. 10a shows a serious Doppler expansion, which decreases the detection performance and the precision of speed estimation. In our simulations, we set the Doppler frequency at $T/2$ as 269 Hz. MDCFT is exploited to compensate for the loss (Fig. 10a). The expansion is rectified and the amplitude of the peak has been improved. The Doppler value after MDCFT is determined by the initial Doppler frequency. Thereby, the target peak in Fig. 10a is centered at the edge of the curve before compensation. With regard to the influence of the discretization, the compensation result after interpolation is shown in Fig. 10b.

Previous simulations have verified the effectiveness of MDCFT for strong targets. Now a weak target affected by noise is simulated in case 1 (Figs. 10c and 10d). The results indicate that MDCFT also works well for weak targets. The SNR is 11.8059 dB after MDCFT compared with the undetectable result before MDCFT.

Moreover, simulations are performed to show the performance of MDCFT for targets with different speeds. Results before and after MDCFT of the targets with different $K_i$ are shown in Figs. 11a and 11c for case 1 and case 2, respectively. The $v_{r,i}\cos(\beta_i/2)$ is a constant 59.7764 m/s for case 1 and 49.7967 m/s for case 2. In Figs. 11b and 11d, the estimated FM rate is compared with the FM rate calculated according to Eq. (14). The estimation error is introduced mainly by the discretization of the FM rate and the noise when performing MDCFT. The fluctuation of the curve is introduced mainly by noise.

In Figs. 10 and 11, the performance of MDCFT is tested on a single target for both cases. Now we simulate a multi-target scenario in case 1. The $v_{r,i}$ and $v_i$ of the three targets are (60, 60) m/s, (60, 680) m/s, (20, 200) m/s. The integration results before compensation are illustrated in Fig. 12. Targets overlap each other. The MDCFT method shows good performance with no need of cross-term consideration (Fig. 13a). Figs. 13b–13d are three cross-sections of

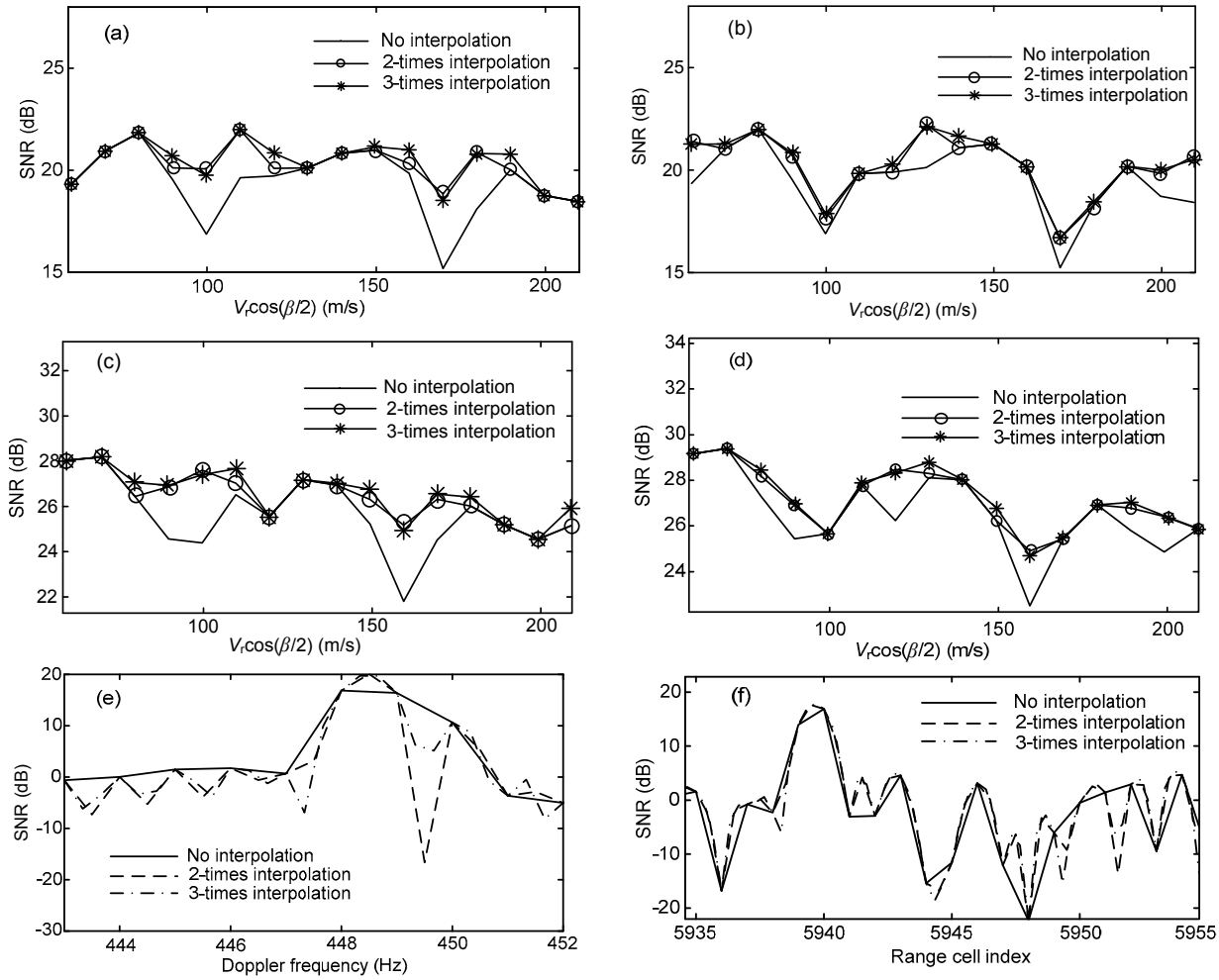


**Fig. 9 The SNR after interpolation**

(a) Case 1: interpolation along the Doppler cells; (b) Case 1: interpolation along the range cells; (c) Case 2: interpolation along the Doppler cells; (d) Case 2: interpolation along the range cells; (e) Case 1: cross-section along the Doppler cells for $v_{r,i}\cos(\beta_i/2)$=99.83 m/s; (f) Case 1: cross-section along range cells for $v_{r,i}\cos(\beta_i/2)$=99.83 m/s

the results. Simulations illustrate that MDCFT is suitable for the multi-target scenario but we should pay attention to the resolution presented in Eq. (18). MDCFT costs 0.0391 s (MATLAB, CPU: i5-2400, no parallelism), when $K_i$ is in the range of [−18, 18] Hz/s and the searching interval is 0.2 Hz/s. However, the RSPWVD-Hough transform costs 27.6706 s. The Doppler shifts reduce to a single value according to Fig. 13. It can also be found that the single Doppler value is equal to that of the initial Doppler during the integration time. This conclusion can also be drawn according to Eq. (14). MDCFT compensates for $\exp(j\pi K_i(mT)^2)$; therefore, the Doppler after the compensation is $f_{d,i}$ (the Doppler frequency at $t_m$=0).

In Section 4.2, a velocity (moving speed and its angle) estimation method has been proposed based on MDCFT. The direction of the velocity is represented by the angle of the moving direction and the connection of the target and the transmitter. The estimation error of $\theta_{r,i}$ is about 2° in the simulations (the estimation precision of the direction of arrival is not very high in passive radar, and 2° is a reasonable parameter for targets around 75 km and 100 km away from the receiver). The actual velocity of the simulated target is 680 m/s with $\varphi_i$=81.2979° in case 1, and 350 m/s with $\varphi_i$=76.6179 in case 2. It can be seen that the estimated velocity depends mainly on the estimation error of $K_i$ (affected by SNR). The estimated velocity with different SNRs (the SNR of targets after MDCFT) are presented in Fig. 14. Results in case 1

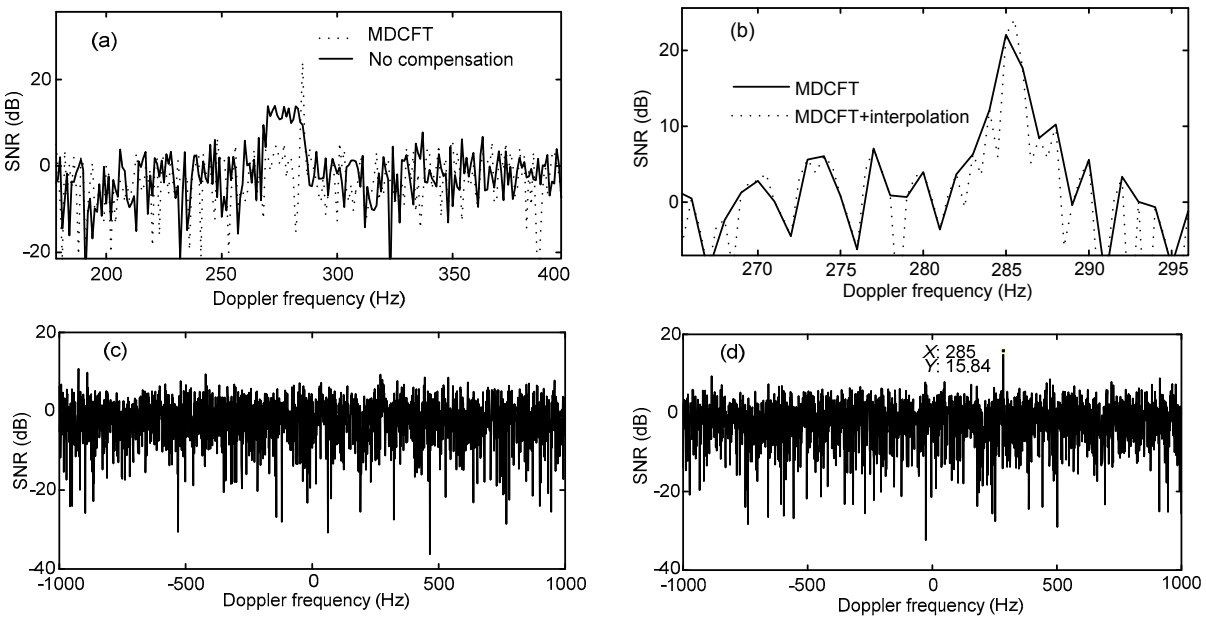


**Fig. 10 The results of MDCFT in case 1**

(a) Comparison of results before and after MDCFT; (b) The results of MDCFT with interpolation; (c) Weak target before compensation; (d) The results of MDCFT for a weak target (the target is marked in the figure)

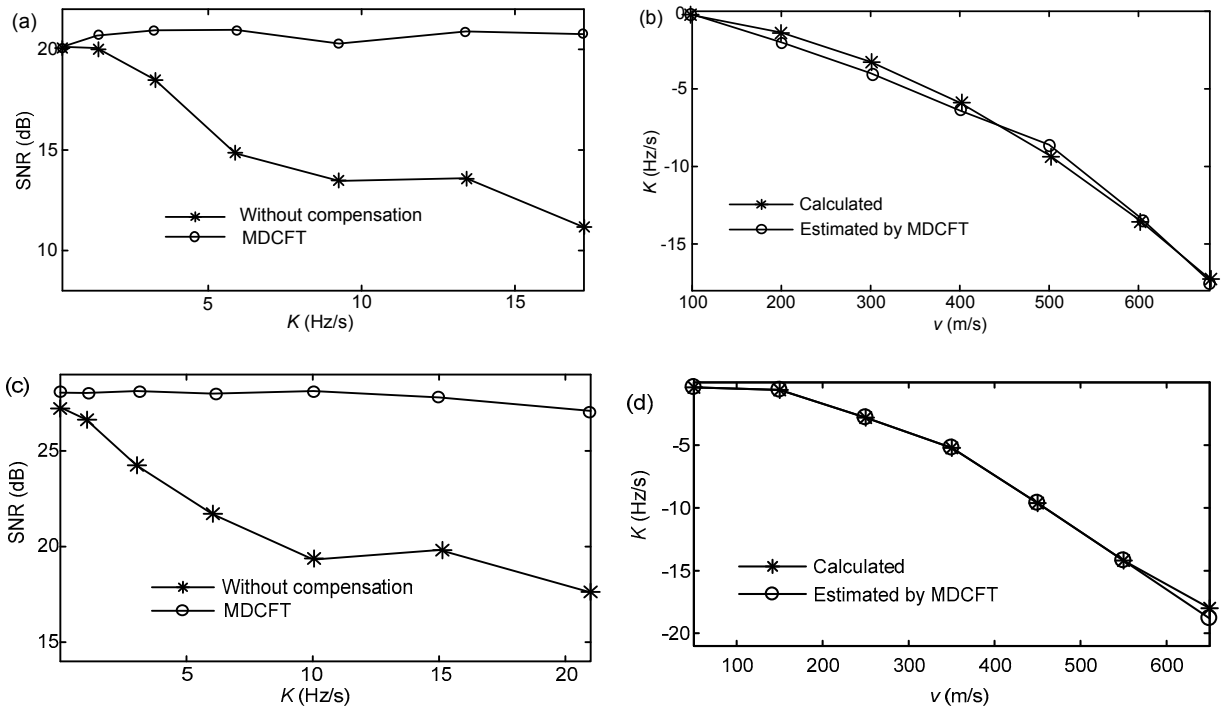


**Fig. 11 The results of MDCFT with different *K*'s**

(a) Case 1: SNR; (b) Case 1: estimated *K*; (c) Case 2: SNR; (d) Case 2: estimated *K*

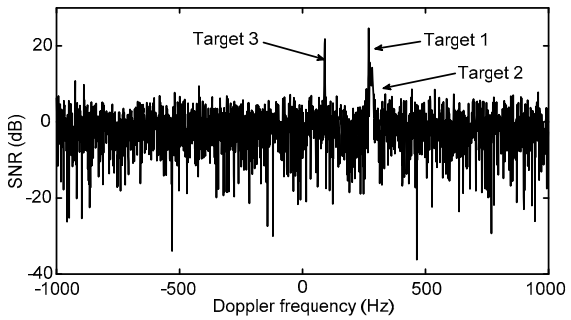


**Fig. 12 Cross-section of the multi-target scenario before compensation**

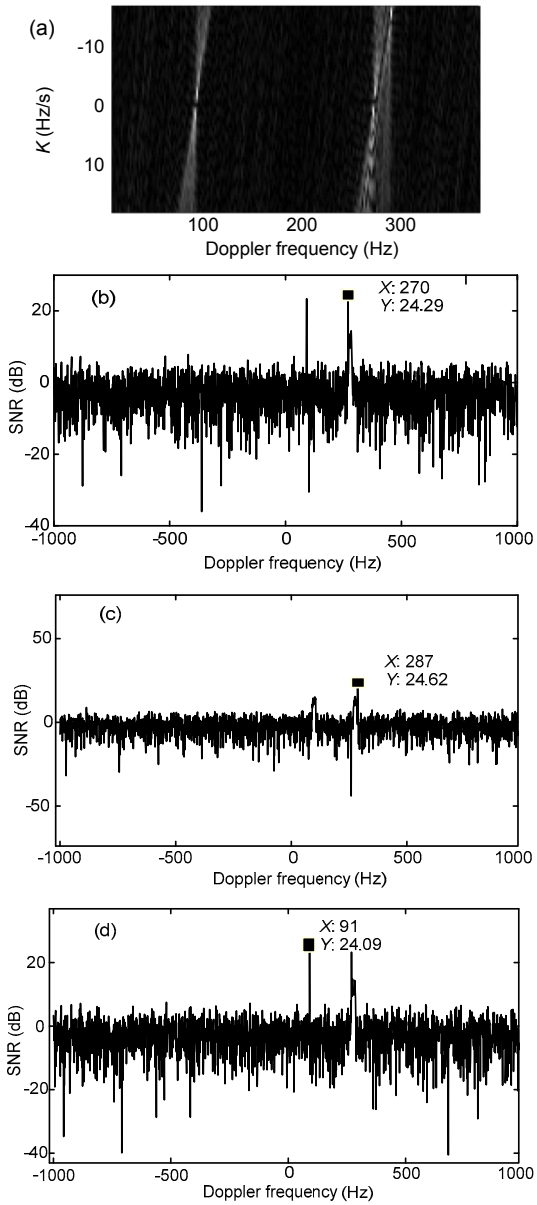


**Fig. 13 MDCFT results for multi-target**
(a) MDCFT analysis; (b) Cross-section of target 1; (c) Cross-section of target 2; (d) Cross-section of target 3

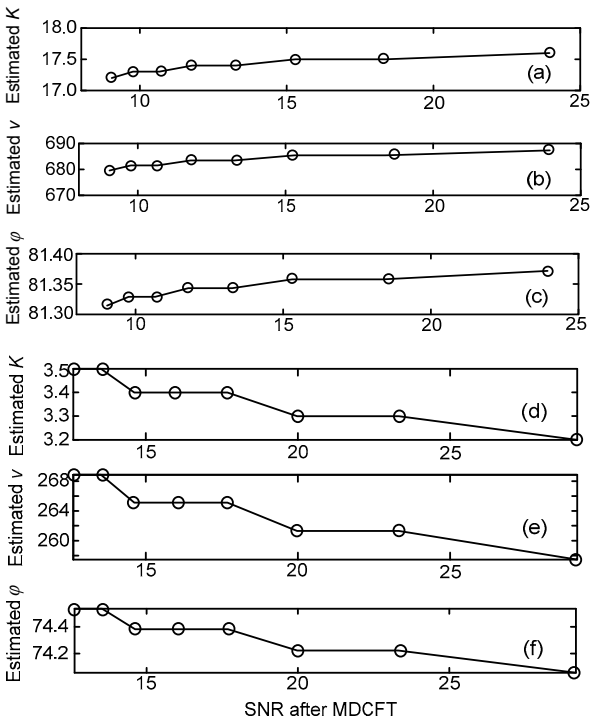


**Fig. 14 Velocity estimation results for different SNR**
(a) Case 1: estimated $K$; (b) Case 1: estimated $v$; (c) Case 1: estimated $\varphi$; (d) Case 2: estimated $K$; (e) Case 2: estimated $v$; (f) Case 2: estimated $\varphi$

are illustrated in Fig. 14a and results in case 2 in Fig. 14b. The estimated velocity is affected by SNR since the estimation precision of $K_i$ is affected by SNR. The estimation results in Fig. 14 show that the proposed estimation method provides a rough estimate of the speed and its angle.

In this section, simulations have been carried out to show the performance of the proposed methods for different $v_{r,i}\cos(\beta_i/2)$ ($K_i$ is around zero) or different $K_i$ with fixed $v_{r,i}\cos(\beta_i/2)$. Two different geometries are discussed. However, the geometry and target parameters affect $v_{r,i}\cos(\beta_i/2)$ and $K_i$, which has not been fully discussed here. Further analyses about the impact of radar geometries and target parameters will be considered in future work.

## 6 Conclusions

In this paper, coherent integration based on matched filtering and keystone transform in passive radar has been investigated by analyzing the impact of mismatching, precision of the keystone implementa-

tion method, discretization, and Doppler expansion. First, the mismatching phenomenon is analyzed and a method based on Doppler filter banks is presented to reduce energy loss. Second, the precision of keystone implementation methods is tested. The chirp-*z* method is proven to be the most effective one, and can be performed in real time. Third, the impact of discretization and interpolation has been discussed. In addition, MDCFT is used to rectify the Doppler expansion, and its performance in multi-target scenarios is analyzed. Finally, a moving speed estimation method with one receiver is proposed for passive bistatic radar. In total, an extended processing scheme is presented for matched filtering based coherent integration in passive radar. The processing scheme can reduce the energy loss to a neglectable amount and can help perform velocity estimation. Further analysis should be undertaken considering target fluctuation and radar geometry.

## References


Auger, F., Flandrin, P., 1995. Improving the readability of time-frequency and time-scale representations by the reassignment method. *IEEE Trans. Signal Process.*, **43**(5): 1068-1089. [doi:10.1109/78.382394]

Barbarossa, S., 1995. Analysis of multi-component LFM signals by a combined Wigner-Hough transform. *IEEE Trans. Signal Process.*, **43**(6):1511-1515. [doi:10.1109/78.388866]

Berger, C., Demissie, B., Heckenbach, J., 2010. Signal processing for passive radar using OFDM waveforms. *IEEE J. Sel. Topics Signal Process.*, **4**(1):226-238. [doi:10.1109/JSTSP.2009.2038977]

Celik, N., Youn, H.S., Omaki, N., *et al*., 2011. Experimental evaluation of passive radar approach for homeland security applications. IEEE Int. Symp. on Antennas and Propagation, p.224-227. [doi:10.1109/APS.2011.5996635]

Cherniakov, M., 2008. Bistatic Radar: Emerging Technology. John Wiley & Sons, West Sussex, England, p.301-302.

Deng, T.D., Jiang, C.S., 2011. Evaluations of keystone transforms using several interpolation methods. IEEE CIE Int. Conf. on Radar, p.1876-1878. [doi:10.1109/CIE-Radar.2011.6159939]

Dong, Y.Q., Tao, R., Zhou, S.Y., *et al*., 1999. Multicomponent chirp signal detection using fractional Fourier analysis. *J. Syst. Eng. Electron.*, **10**(3):57-63.

Griffiths, H.D., 2011. Developments in bistatic and networked radar. IEEE CIE Int. Conf. on Radar, p.10-13. [doi:10.1109/CIE-Radar.2011.6159708]

Guo, X., Sun, H.B., Wang, S.L., *et al*., 2002. Comments on "Discrete chirp-Fourier transform and its application to chirp rate estimation". *IEEE Trans. Signal Process.*, **50**(12):3115. [doi:10.1109/TSP.2002.805492]

Howland, P., 2005. Passive radar systems. *IEE Proc.-Radar Sonar Navig.*, **152**(3):105-106. [doi:10.1049/ip-rsn:20059064]

Howland, P., Maksimiuk, D., Reitsma, G., 2005. FM radio based bistatic radar. *IEE Proc.-Radar Sonar Navig.*, **152**(3):107-115. [doi:10.1049/ip-rsn:20045077]

Li, Y., Zeng, T., Long, T., *et al.*, 2006. Range migration compensation and Doppler ambiguity resolution by keystone transform. IEEE CIE Int. Conf. on Radar, p.1-4. [doi:10.1109/ICR.2006.343404]

Liu, L., Tao, R., Zhang, N., 2011. The CAF-DFRFT-KT algorithm for high-speed target detection in passive radar. Int. Conf. on Instrumentation, Measurement, Computer, Communication and Control, p.748-751. [doi:10.1109/IMCCC.2011.190]

Malanowski, M., 2012. Detection and parameter estimation of manoeuvring targets with passive bistatic radar. *IET Radar Sonar Navig.*, **6**(8):739-745. [doi:10.1049/iet-rsn.2012.0072]

Malanowski, M., Kulpa, K., Olsen, K.E., 2011. Extending the integration time in DVB-T based passive radar. Proc. 8th European Radar Conf., p.190-193.

National Standardization Committee of China, 2006. GB 20600-2006. Framing Structure, Channel Coding and Modulation for Digital Television Terrestrial Broadcasting System (in Chinese).

Palmer, J., Palumbo, S., Summers, A., *et al*., 2011. An overview of an illuminator of opportunity passive radar research project and its signal processing research directions. *Dig. Signal Process.*, **21**(5):593-599. [doi:10.1016/j.dsp.2011.01.002]

Palmer, J., Harms, A., Searle, S.J., *et al.*, 2013. DVB-T passive radar signal processing. *IEEE Trans. Signal Process.*, **61**(8):2116-2126. [doi:10.1109/TSP.2012.2236324]

Petri, D., Moscardini, C., Martorella, M., *et al.*, 2012. Performance analysis of the batches algorithm for range-Doppler map formation in passive bistatic radar. IET Int. Conf. on Radar Systems, p.1-4. [doi:10.1049/cp.2012.1570]

Xia, X.G., 2000. Discrete chirp-Fourier transform and its application to chirp rate estimation. *IEEE Trans. Signal Process.*, **48**(11):3122-3133. [doi:10.1109/78.875469]

Yardley, H.J., 2007. Bistatic radar based on DAB illuminators: the evolution of a practical system. IEEE Radar Conf., p.688-692. [doi:10.1109/RADAR.2007.374302]

Zhao, Z.X., Wan, X.R., Zhang, D.L., *et al*., 2013. An experimental study of HF passive bistatic radar via hybrid sky-surface wave mode. *IEEE Trans. Antennas Propag.*, **61**(1):415-424. [doi:10.1109/TAP.2012.2213062]

Zhu, D.Y., Li, Y., Zhu, Z.D., 2007. A keystone transform without interpolation for SAR ground moving-target imaging. *IEEE Geosci. Remote Sens. Lett.*, **4**(1):18-22. [doi:10.1109/LGRS.2006.882147]